Bull. Mater. Sci., Vol. 40, No. 6, October 2017, pp. 1285–1289
DOI 10.1007/s12034-017-1451-8

Bipolar resistive switching behaviour in $Mn_{0.03}Zn_{0.97}O$/amorphous $La_{0.7}Zn_{0.3}MnO_3$ heterostructure films

HUA WANG*, QISONG CHEN, JIWEN XU, XIAOWEN ZHANG and SHUAISHUAI YAN
School of Materials Science and Engineering, Guilin University of Electronic Technology, Guilin, China
*Author for correspondence (wh65@tom.com)

MS received 14 October 2016; accepted 30 January 2017; published online 9 September 2017

Abstract. $Mn_{0.03}Zn_{0.97}O$ (MZO)/amorphous $La_{0.7}Zn_{0.3}MnO_3$ (LZMO) heterostructures were deposited on p^+-Si substrates through sol–gel spin coating. Ag/MZO/LZMO/p^+-Si and Ag/LZMO/MZO/p^+-Si devices exhibit a bipolar, reversible and remarkable resistive switching behaviour at room temperature. The ratio of the resistance at high-resistance state (HRS) to that at low-resistance state (LRS) (R_{HRS}/R_{LRS}) in the Ag/LZMO/MZO/p^+-Si device is approximately five orders of magnitude, and is maintained after over 10^3 successive switching cycles or over a period of 2×10^6 s, indicating good endurance property and retention characteristics. Conversely, the ratio in the Ag/MZO/LZMO/p^+-Si device began to decrease after 100 successive switching cycles. The LZMO/MZO interface could play an important role in the resistive switching behaviour of the devices. The dominant conduction mechanism of the two devices is charge-trap emission.

Keywords. $Mn_{0.03}Zn_{0.97}O$; amorphous $La_{0.7}Zn_{0.3}MnO_3$; heterostructures; resistive switching; sol–gel.

1. Introduction

Considering that traditional flash memories rapidly approach their physical downsizing limitations, researchers have focused on resistive random access memory (RRAM) because of its excellent scalability, simple structure, superior performance, low operation voltage, low power consumption, high-speed operation and long retention [1–4]. Various materials, such as perovskite oxides ($Re_{1-x}A_xMnO_3$ [5–7] and $SrZrO_3$ [8]), binary metal oxides (ZnO [9], ZrO_2 [10] and NiO [11]), amorphous materials [12–14] and organic materials [15], have been reported to possess resistive switching behaviour. The resistive switching properties of perovskite $Re_{1-x}A_xMnO_3$ (Re = Pr, La; A = Ca, Sr) thin films have been extensively investigated [7]. Although devices consisting of $Re_{1-x}A_xMnO_3$ exhibit endurance properties, their resistance ratio (R_{HRS}/R_{LRS}) is low [5,6]. By contrast, devices with Mn-doped ZnO feature poor endurance properties but good resistive switching performance [16].

Transforming the structure of resistive switching devices is an effective method used to enhance resistive switching properties. In this work, $Mn_{0.03}Zn_{0.97}O$ (MZO)/amorphous $La_{0.7}Zn_{0.3}MnO_3$ (LZMO) heterostructures were developed to enhance resistive switching characteristics and endurance properties.

2. Experiments

MZO/LZMO thin films were fabricated on p^+-Si substrates through sol–gel spin coating. LZMO solution was synthesized using $La(NO_3)_3 \cdot 6H_2O$, $Zn(CH_3COO)_2 \cdot 2H_2O$ and $Mn(CH_3COO)_2 \cdot 4H_2O$ as source materials, absolute 2-methoxyethanol as solvent and diethanolamine as stabilizer. MZO solution was synthesized using $Mn(CH_3COO)_2 \cdot 4H_2O$ and $Zn(CH_3COO)_2 \cdot 2H_2O$ as source materials, 2-methoxyethanol and isopropanol as solvents and cholamine as stabilizer. LZMO films were prepared on (100)-oriented p^+-Si substrates through spin coating, whereas MZO films were prepared through spin coating and then preheated at 350°C to remove the solvent and organics. Finally, the films were annealed at 600°C for 1 h. Ag (work function: 4.26 eV) was deposited on the substrate with a diameter of 200 μm as the top electrode to fabricate Ag/MZO/LZMO/p^+-Si devices. Furthermore, the deposition order of LZMO and MZO films was exchanged to fabricate Ag/LZMO/MZO/p^+-Si devices.

The crystalline phases of the thin films were characterized by X-ray diffraction (XRD, AXS D8-ADVANCE, Bruker) analysis. The surface morphologies were observed through atomic force microscopy (AFM, SPI3800N, Seiko) and scanning electron microscopy (SEM, S4800, Hitachi). Current–voltage ($I-V$) curves were obtained using a digital source meter (2400, Keithley) at room temperature.

3. Results and discussion

The XRD patterns of MZO/LZMO/p^+-Si and LZMO/MZO/p^+-Si are shown in figure 1. Except for the characteristic peaks of the p^+-Si substrate, only the characteristic peak of the (002) plane belongs to the ZnO crystal and conforms to PDF card No. 36-1451. No characteristic peaks

of crystalline LZMO were observed, demonstrating that the LZMO films possess an amorphous structure. Moreover, no characteristic peaks of crystalline ZnO were observed in the LZMO/MZO/p^+-Si XRD pattern. Hence, the LZMO films possibly impede X-rays in detecting the ZnO crystal.

Figure 2a shows the three-dimensional surface morphology of MZO/LZMO/p^+-Si by AFM, with uniform grain diameter (30–50 nm) and a roughness of 1.23 nm. By contrast, no crystalline grains with a roughness of 0.42 nm were observed on the surface of the films consisting of LZMO/MZO/p^+-Si (figure 2b). This finding is consistent with the result showing that the LZMO films are amorphous. The cross-sectional morphologies of MZO/LZMO/p^+-Si and LZMO/MZO/p^+-Si by SEM are shown in figure 2c and d, respectively. Figure 2 reveals that the LZMO and MZO films are dense, and all of their layers are well stacked upon each other. Moreover, the boundaries between crystalline MZO and amorphous LZMO, between crystalline MZO and p^+-Si substrates, and between amorphous LZMO and p^+-Si substrates are clear. All boundaries show cohesion, and the thicknesses of MZO/LZMO and LZMO/MZO are 230 and 239 nm, respectively.

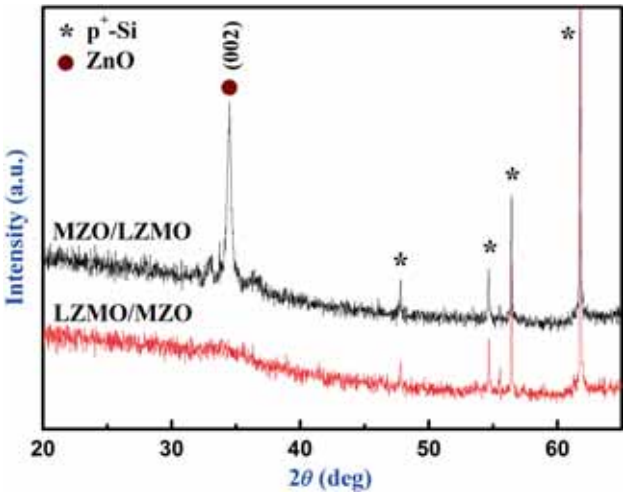

Figure 1. XRD patterns of the LZMO/MZO and the MZO/LZMO thin films deposited on p^+-Si substrates.

When a voltage bias swept as $0 \rightarrow +U \rightarrow 0 \rightarrow -U \rightarrow 0$ cycle was applied to the devices, a typical bipolar resistive switching behaviour was observed in the two structures through the I–V curve described in figure 3. Unlike devices based on ZnO and $Re_{1-x}A_xMnO_3$, the devices fabricated in the present study are in low-resistance state (LRS) when a forward bias is applied. The state switches from LRS to high-resistance state (HRS) when the bias increases to V_{set} in the voltage sweep 1 ($0 \rightarrow +U$); meanwhile, the state is converted from HRS to LRS at V_{reset} in the voltage sweep 2 ($+U \rightarrow 0 \rightarrow -U$). In addition, the ratio of the resistance at HRS to that at LRS (R_{HRS}/R_{LRS}) in the Ag/LZMO/MZO/p^+-Si device can be easily obtained; the ratio was found to be approximately 10^5–10^6,

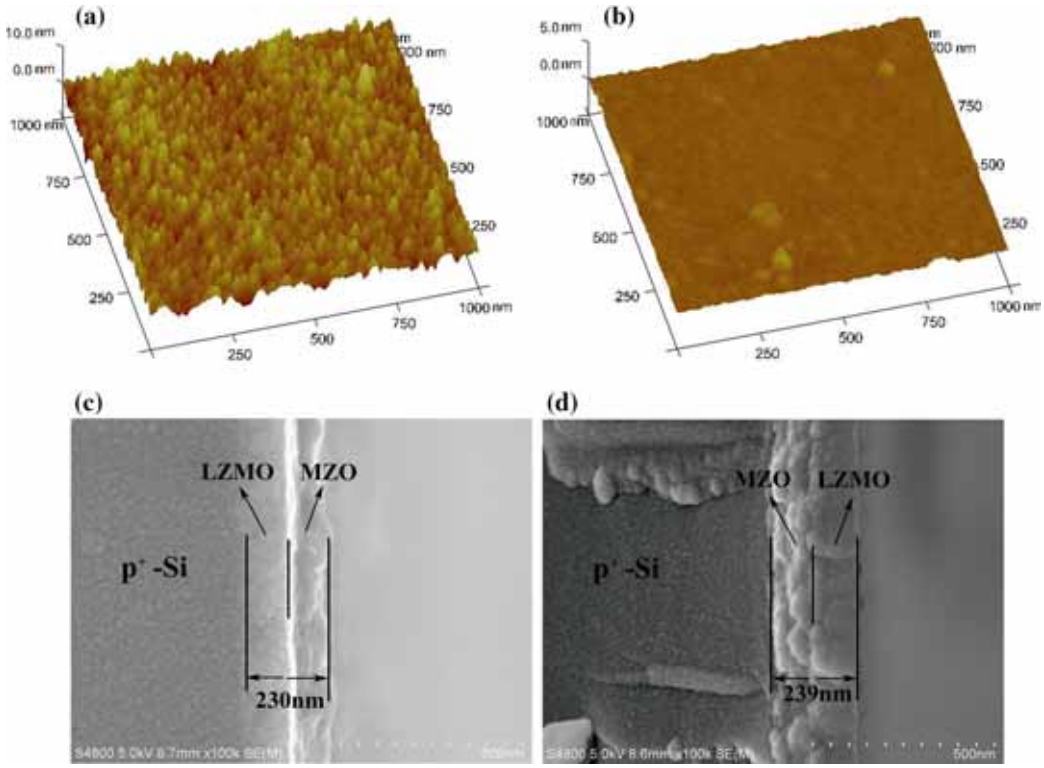

Figure 2. Three-dimensional surface AFM images and cross-sectional SEM images of the films: (**a**, **c**) MZO/LZMO/p^+-Si and (**b**, **d**) LZMO/MZO/p^+-Si.

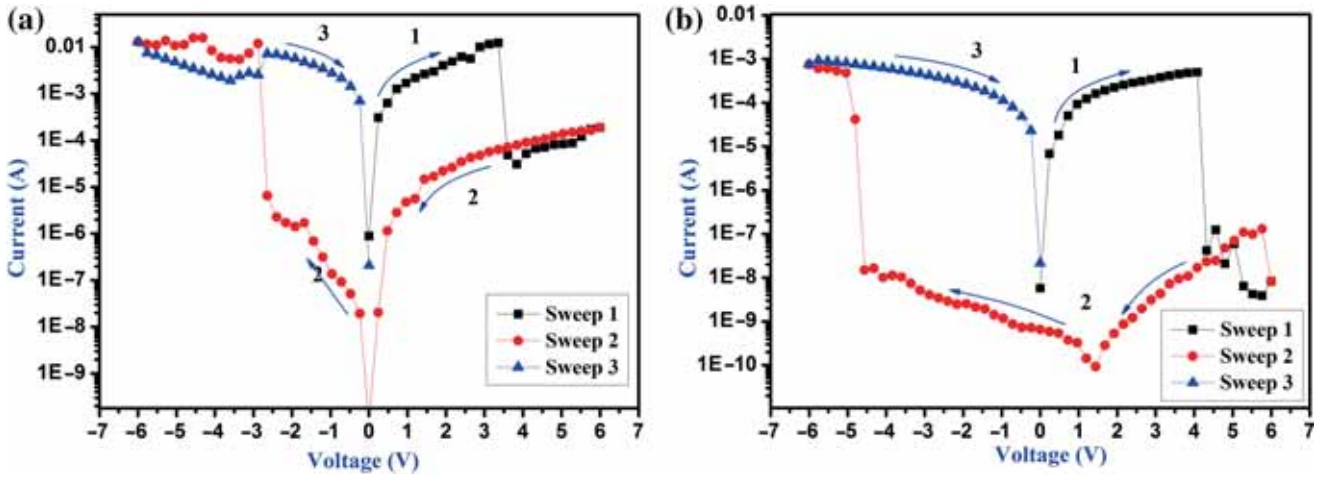

Figure 3. I–V characteristics of the devices: (**a**) Ag/MZO/LZMO/p$^+$-Si and (**b**) Ag/LZMO/MZO/p$^+$-Si.

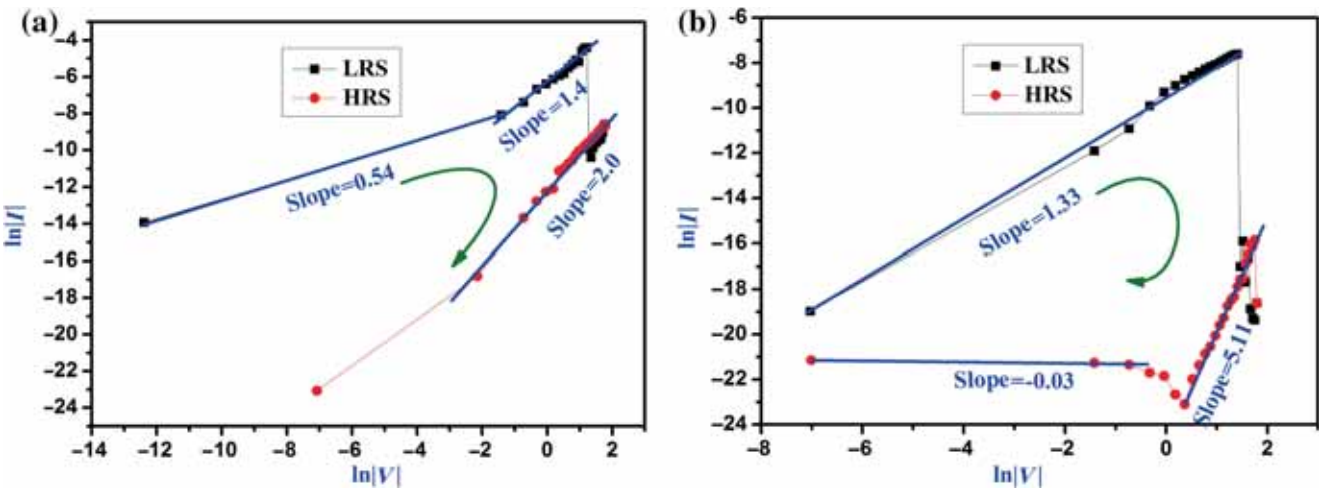

Figure 4. Positive I–V curve of the devices plotted in ln|I|–ln|V| scale curves: (**a**) Ag/MZO/LZMO/p$^+$-Si and (**b**) Ag/LZMO/MZO/p$^+$-Si.

which is higher than that in the Ag/MZO/LZMO/p$^+$-Si device.

The positive I–V curves of the devices in the ln|I|–ln|V| scale were obtained and are shown in figure 4 to clarify the conduction mechanism. The arrow shows the voltage sweeping direction. Based on the initial feature of LRS, the charge-trap emission [17,18] was speculated to be the dominant mechanism of the two devices. When a forward bias was applied to the devices, injection carriers were captured by the traps and used to build an interior electric field. The number of trapped carriers increases with increasing applied voltage; thus, field strength also increases. When the interior field strength becomes higher than the applied field strength, the resistance increases rapidly and setting occurs. When negative voltage is applied, the trapped carriers are ejected; subsequently, the conductivity increases, which corresponds to the setting process. The devices generally contain two types of traps: naturally formed traps, such as dislocation, grain boundary and oxygen vacancies; and interface between the LZMO and the MZO films, as well as between the films and the trades, which differ because of the deposition order of the two films. Dislocation and grain boundary cannot be precisely controlled to obtain uniform growth; hence, these phenomena are not the reasons for the resistive switching behaviour. The deposition order of the two films is not the reason for charge-trap emission, as the films obey the same charge-trap emission. By contrast, oxygen vacancies and interface traps may contribute to the resistive switching behaviour. The dominant conduction mechanisms in devices based on $LaMnO_3$ [6] and ZnO [9] include the Schottky barrier and conduction filaments, which are controlled by oxygen vacancies and are not the reason for charge-trap emission in the devices. Thus, controllable interface traps between the LZMO and MZO films contribute to the charge-trap emission. Deposition order and

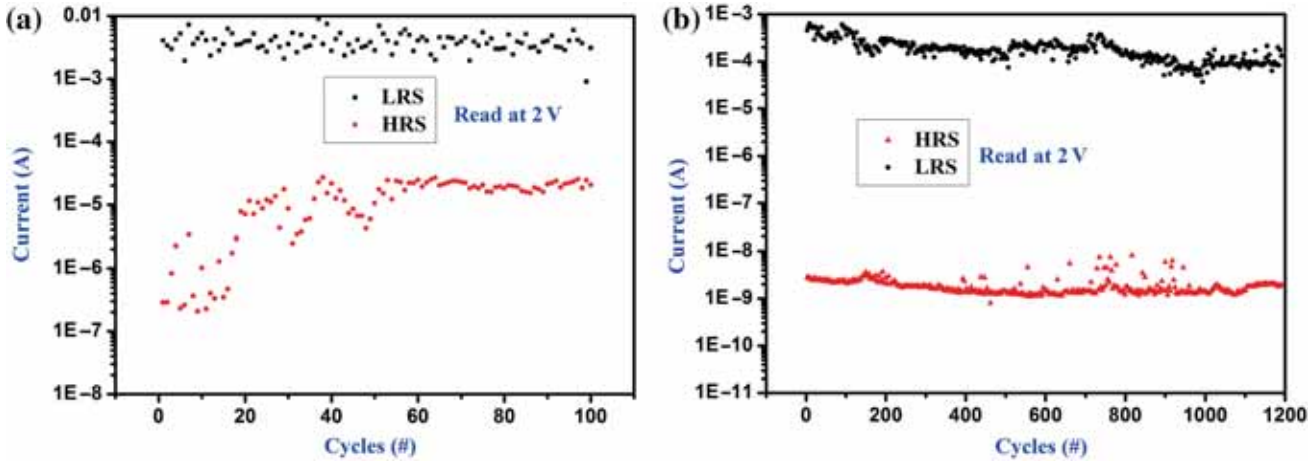

Figure 5. Endurance performance of the devices: (**a**) Ag/MZO/LZMO/p^+-Si and (**b**) Ag/LZMO/MZO/p^+-Si.

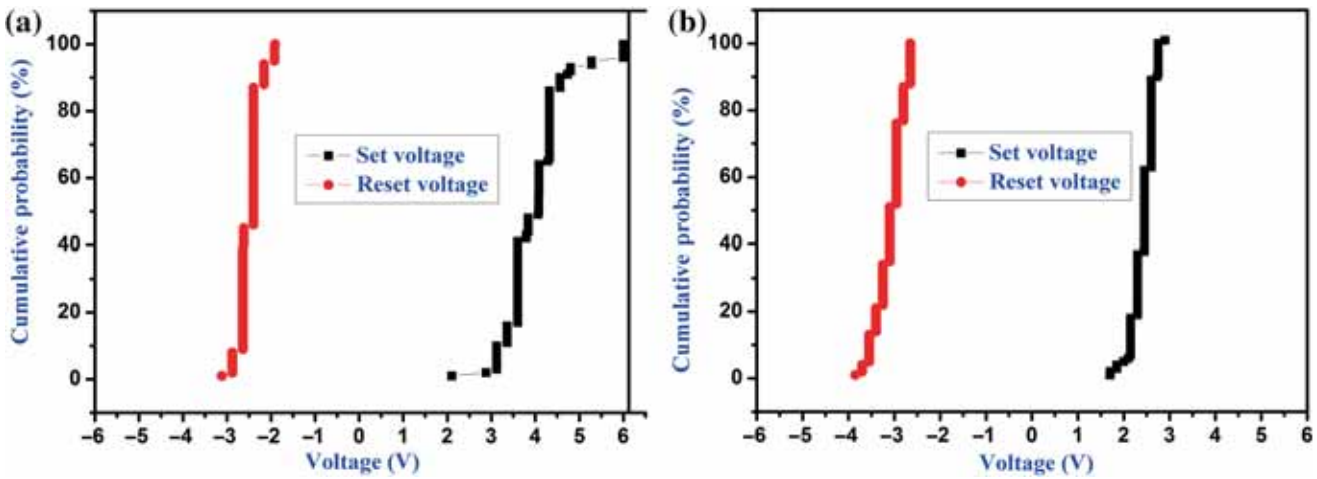

Figure 6. V_{set} and V_{reset} distributions: (**a**) Ag/MZO/LZMO/p^+-Si and (**b**) Ag/LZMO/MZO/p^+-Si.

oxygen vacancies lead to different slopes of the fitting line (figure 4).

I–V cycling test was conducted to evaluate the endurance property of the devices, and the results are shown in figure 5. From figure 5a, it can be seen that the R_{HRS}/R_{LRS} ratio of Ag/MZO/LZMO/p^+-Si device decreases from 10^4 to 10^2 with the switching cycle up to the 50th, and is maintained for about 10^4 s. Figure 5b shows that the R_{HRS}/R_{LRS} ratio of Ag/LZMO/MZO/p^+-Si device remains high (10^5–10^6) over 10^3 switching cycles. In addition, the resistance values of LRS or HRS of Ag/LZMO/MZO/p^+-Si device remained almost unchanged over a period of 2×10^6 s, indicating good retention property. The poor endurance properties and retention characteristics in Ag/MZO/LZMO/p^+-Si device may be ascribed to the poor quality of MZO grown on the amorphous LZMO film.

Writing and erasing data can be easily controlled when the V_{set} and V_{reset} of the RRAM devices are stable. Figure 6 depicts the V_{set} and V_{reset} distributions of the two devices. The V_{set} and V_{reset} of the Ag/LZMO/MZO/p^+-Si device demonstrate narrow distributions ranging from 1.5 to 2.8 and from −2.7 to −3.9 V, respectively, in the forward 350 cycles; this finding indicates the stable SET and RESET processes. By contrast, the V_{reset} of the Ag/MZO/LZMO/p^+-Si device shows narrow distributions ranging from −2.0 to −3.4 V, whereas the V_{set} is distributed through a large range of 2–6 V. The V_{set} distribution of the Ag/MZO/LZMO/p^+-Si device reveals instability, which is consistent with the result of the analysis on endurance performance.

4. Conclusions

The XRD patterns and SEM images of the two devices reveal that the amorphous LZMO films and the crystalline MZO films are dense and closely packed with each other.

The Ag/LZMO/MZO/p^+-Si device exhibits a bipolar resistive switching behaviour with a high R_{HRS}/R_{LRS} ratio of 10^5–10^6 without any degradation over 10^3 cycles or over a period of 2×10^6 s, and stable V_{set} and V_{reset} distributions, which indicated that the Ag/LZMO/MZO/p^+-Si device has good endurance property and retention characteristics. Moreover, the poor growth of MZO films on amorphous LZMO films is responsible for the poor endurance property and retention characteristics of the Ag/MZO/LZMO/p^+-Si device. Furthermore, the conduction mechanism of the two devices is the charge-trap emission.

Acknowledgements

This work has been financially supported by Natural Science Foundation of China (Grant Number 51262003) and Guangxi Key Laboratory of Information Materials (Guilin University of Electronic Technology), China (Project Number 1110908-10-Z).

References

[1] Waser R and Aono M 2007 *Nature* **6** 883
[2] Waser R, Dittmann R, Staikov G and Szot K 2009 *Adv. Mater.* **21** 2632
[3] Kozicki M N, Mira P and Maria M 2005 *IEEE Trans. Nanotechnol.* **4** 331
[4] Russo U, Kamalanathan D, Ielmini D, Lacaita A L and Kozicki M N 2009 *IEEE Trans. Electron Dev.* **56** 1040
[5] Dong R, Wang Q, Chen L D, Shang D S, Chen T L, Li X M *et al* 2005 *Appl. Phys. Lett*. **86** 172107–1
[6] Xu Z T, Jin K J, Gu L, Jin Y L, Ge C, Wang C *et al* 2012 *Small* **8** 1279
[7] Wang H, Li Z, Xu J, Zhang Y, Yang L and Qiu W 2015 *J. Wuhan Univ. Technol.—Mater. Sci.* **30** 1159
[8] Beck A, Bednorz J G, Gerber C, Rossel C and Widmer D 2000 *Appl. Phys. Lett.* **77** 139-1
[9] Tang M H, Zeng Z Q, Li J C, Wang Z P, Xu X L, Wang G Y *et al* 2011 *Solid-State Electron*. **63** 100
[10] Liu Q, Guan W, Long S, Jia R, Liu M and Chen J 2008 *Appl. Phys. Lett.* **92** 012117-1
[11] Son J Y and Shin Y H 2008 *Appl. Phys. Lett.* **92** 222106-1
[12] Seong T G, Choi K B, Seo I T, Oh J H, Moon J W, Hong K *et al* 2012 *Appl. Phys. Lett.* **100** 212111-1
[13] Jo S H, Kim K H and Lu W 2009 *Nano Lett*. **9** 870
[14] Liu D Q, Wang N N, Wang G, Shao Z Z, Zhu X, Zhang C Y *et al* 2013 *Appl. Phys. Lett.* **102** 134105-1
[15] Scott J C and Bozano L D 2007 *Adv. Mater*. **19** 1452
[16] Yang Y C, Pan F, Liu Q, Liu M and Zeng F 2009 *Nano Lett*. **9** 1636
[17] Lee D, Choi H J, Sim H J, Choi D, Hwang H, Lee M J *et al* 2005 *IEEE Electron Dev. Lett.* **26** 719
[18] Guan W H, Long S B, Jia R and Liu M 2007 *Appl. Phys. Lett.* **91** 062111-1